

Fault reactivation induced by tunneling activity in clay material: Hints from numerical modeling

Journal Article**Author(s):**

Rinaldi, Antonio P.; Urpi, Luca

Publication date:

2020-08

Permanent link:

<https://doi.org/10.3929/ethz-b-000417004>

Rights / license:

[Creative Commons Attribution-NonCommercial-NoDerivatives 4.0 International](#)

Originally published in:

Tunnelling and Underground Space Technology 102, <https://doi.org/10.1016/j.tust.2020.103453>

Funding acknowledgement:

160555 - To induce or not to induce: an open problem. Study on injection-induced seismicity for GeoEnergy applications, from lab to field scale (SNF)

FAULT REACTIVATION INDUCED BY TUNNELING
ACTIVITY IN CLAY MATERIAL: HINTS FROM
NUMERICAL MODELING

Antonio P. Rinaldi & Luca Urpi

Swiss Seismological Service, Swiss Federal Institute of Technology, ETHZ, Zurich,
Switzerland

e-mail: antoniopio.rinaldi@sed.ethz.ch, luca.urpi@sed.ethz.ch

(*) Corresponding author at: Swiss Seismological Service, ETHZ, Sonneggstrasse 5, Zurich,
Switzerland

submitted to Tunneling and Underground Space Technology

ABSTRACT

Seismic events with magnitude 3 and above have been associated with the removal of rock mass in mining environment since long-time. On the contrary, little is known about the possible seismic events induced by tunneling, although it presents similarities with mining. One great example is the case of the 57 km long Gotthard Base Tunnel excavation, which has been associated more than hundred seismic events, with the largest one having magnitude of ML 2.4, damaging the tunnel infrastructures (e.g. gallery floor or portal area). Different underground structures will be built probably up to 1000 m below ground for the construction of future deep geological for the storage of nuclear waste. While seismic risk will probably not constitute a liability for the storage site construction, it is important to understand the potential for reactivation of seismogenic features located nearby the future location of emplacement tunnels. Here we present numerical simulations aimed at understanding the potential for fault reactivation during tunnel construction in clay material, a potential host rock for nuclear waste repository. We evaluate the evolution of the stress changes during the simulation of the excavation with FLAC3D numerical solver. A strain-softening friction model is used to simulate the occurrence of a sudden slip on a fault zone when critical conditions for reactivation are satisfied. This constitutes a worst-case scenario, given the low seismogenic potential of clay rocks. We also present a sensitivity analysis on several critical parameters including fault frictional properties, stress conditions, as well as different tunnel sizes at varying distance from a nearby failure plane, with the final purpose of evaluating safety of a potential nuclear repository site on the short- and long-term.

Keywords: tunnel excavation, fault reactivation, induced seismicity, geomechanical modeling, geological nuclear repositories

1. INTRODUCTION

Human activities in the underground are nowadays frequently associated to reactivation of fault zones and induced seismicity (McGarr et al., 2002; Ellsworth et al., 2015; Grigoli et al., 2017). The possible causes of induced seismicity may be grouped into two main categories:

- Hydrological changes, where variation of pore pressure and/or temperature affect the state of stress. Most of the known induced seismicity falls in this category, including large earthquakes because wastewater disposal (e.g. Mw 5.8 Pawnee, Oklahoma, USA – Langenbruch and Zoback, 2016), enhanced geothermal systems (Mw 5.5 Pohang, South Korea – Grigoli et al., 2018), hydrocarbon extraction (Ms 7.0 Gazli,

Uzbekistan, although controversial – Suckale, 2009), as well as reservoir impoundment (ML 6.5 Konya, India – McGarr et al., 2002).

- Removal of physical support (e.g. mining), where the reactivation of an affected fault zone is theoretically related to the physical strength of the rock. Maximum observed magnitudes as high as ML 5.5 for such cases are reported by McGarr et al. (2002).

Seismicity caused by the removal of rock (or fluid) is physically explained by a change in deformation and the state of stress caused by the removal itself. Nearby fault zones may get reactivated due to the stress changes, which can be elastic or poro-elastic. In the first case the change in stress is relatively fast; it occurs as soon as the rock is removed, as a consequence of the need to rebalance the mechanical equilibrium (e.g. Lu et al., 2019). In the second case changes in the state of stress take longer, as the reaction to the perturbation not only occurs as mechanical rebalancing but also as pore- fluid redistribution within the newly deformed rock matrix (Giraud et al., 1993; Anagnostou, 1995; Rutqvist et al., 2009).

Removal of rock mass in mining environment has been associated since long-time with seismic event of magnitude 3 and above, with the potential to cause damage to the infrastructures or even loss of human life (McGarr et al., 2002). Although with similarities with mining, relatively unknown up to now are seismic events induced by tunneling. However, with modern mechanized tunneling techniques, making possible to digging deeper and longer underground infrastructure, the risk is not negligible. For example, the construction phase of a high-level waste repository requires the excavation of several tunnels. On the one hand, these tunnels are needed to reach the target formation at depth; on the other hand, a geological repository will feature access as well as emplacement tunnels. Tunnel excavations are known to perturb the hosting rock mass at long distances, with changes in the hydrogeological flow affecting or even draining natural springs, as well as deforming the rock mass, inducing subsidence in a zone above the tunnel (Chou and Bobet,

2002; Mezger et al., 2013; Loew et al., 2015). Predictive, numerical and analytical models, however, show that the accuracy of the calculations can be largely affected by the reliability of the used 3D geological models and by the knowledge of the in-situ effective stress (Preisig et al., 2014).

While several numerical models have been proposed for the deformation of the excavated tunnel and/or for the excavation front (e.g. Rutqvist et al., 2009; Zhao et al., 2010), modeling of fault reactivation linked to tunneling are rare in literature. For example, Stiros and Kontogianni (2009) proposed the use of Coulomb static stress changes to understand possible chain-reaction failure of the rock mass. Indeed, the failure of weak section during the excavation could lead to increases in stress that could propagate and trigger further failure away from the excavation front. A more detailed numerical study about rock failure in the vicinity of a tunnel was provided by Khademian et al., (2016). They conclude that the kinetic energy released by unstable failure highly depends on the lower horizontal to vertical stress ratio. The results for a 2D model of a circular tunnel were also extended to the case of excavation near a fault zone, and a sensitivity analysis on the parameters shows high dependency on the stress ratio, rock stiffness, and tunnel size.

Here we present a similar configuration, but we extend the modeling of a circular tunnel excavation to three dimensions, allowing for a more detailed description of the area affected by plastic strain accumulation. Furthermore, we extend the sensitivity analysis to fault frictional parameters, to better evaluate the potential for induced events in a more “seismological” context. Numerical simulations aim at understanding the potential for inducing seismicity during tunnel construction, with the final purpose of evaluating safety during the construction of a potential nuclear repository in clay material according to the Swiss concept (NAGRA, 2016).

2. CASES OF INDUCED SEISMICITY BY TUNNELING

In comparison with the much more commonly observed seismicity caused by usually deep mining activities, with magnitudes up to 5 (e.g. South African gold field in the Klerksdorp mining district – McGarr et al., 2002), earthquakes induced by road or access tunnel excavations are less common or often go undetected. Indeed, only few cases of tunneling-induced seismicity are documented in literature. An example worth of note is the case of the excavation of the 57 km- long Gotthard Base Tunnel. The drilling of the southern section of the tunnel induced more than hundred micro-earthquakes, with the largest event being recorded near Faido reaching a local magnitude of ML 2.4 (Fig. 1 –Husen et al., 2013). The removal of physical support due to the excavation was interpreted to be responsible for a decrease of the local minimum principal stress on a fault zone striking parallel to the direction of excavation. This earthquake, although of relatively small magnitude, was responsible for relevant damage in the tunnel and delay of the excavation work.

A similar failure during tunnel excavation was recorded at a pilot tunnel, excavated for the Brenner Base Tunnel (Quick et al., 2010). In this case, seismic monitoring was missing, making the determination of the event's magnitude impossible. Strain-meters showed a slow increase in deformation starting on the 6th of August, 2009 and an abrupt large deformation occurred on the 10th of August 2009. This failure caused damage to the tunneling machine and a more than three-month delay. The rupture mechanism is thought by Quick et al., (2010) to be associated with a sudden shear-slip that took place on an undetected vertical fault plane, running parallel to and at a short distance from the tunnel.

Both aforementioned examples feature similar event magnitudes causing damage to the tunnel wall and a similar (granitic/gneissic) environment characterizes them. Furthermore, the overburden thicknesses at the two tunnels was 1000-1500 meters, indicating a possible large differential stress. An example of seismicity induced by tunneling in a shallower

environment (at about 400 m depth) can be found at the Underground Research Laboratory in southeastern Manitoba, Canada (Martin and Chandler, 1996; McGarr et al., 2002; Martino and Chandler, 2004). While also located in granitic rock, seismicity was recorded during the excavation of both shafts and tunnels at different depth levels with magnitudes ranging between -4 and -1.8, i.e. much smaller than in the Alpine base tunnels. A final example of seismicity caused by tunneling in shallower environment is the case of the Mont Terri Underground Rock Laboratory in Switzerland (300 m depth). This example is particularly relevant to the geological repositories since the host rock is clay-rich material, ideal for the disposal of high-level waste. At Mont Terri, several hundred microevents were recorded during the excavation of a gallery in 2008 (Le Gonidec et al., 2014; Amann et al., 2018). The magnitudes of the recorded induced micro-earthquakes range between -0.9 and -0.2. Worth mentioning that for the case of Mont Terri, the microseismic events were recorded at the front of the excavation front, hence possibly related to reactivation of small features rather than failure of the main fault zone. During a more recent excavation at Mont Terri, in 2019, a 3D displacement sensor (Guglielmi et al., 2013) recorded the Main Fault movement, but the analysis of the dataset is currently ongoing (Yves Guglielmi, personal communication).

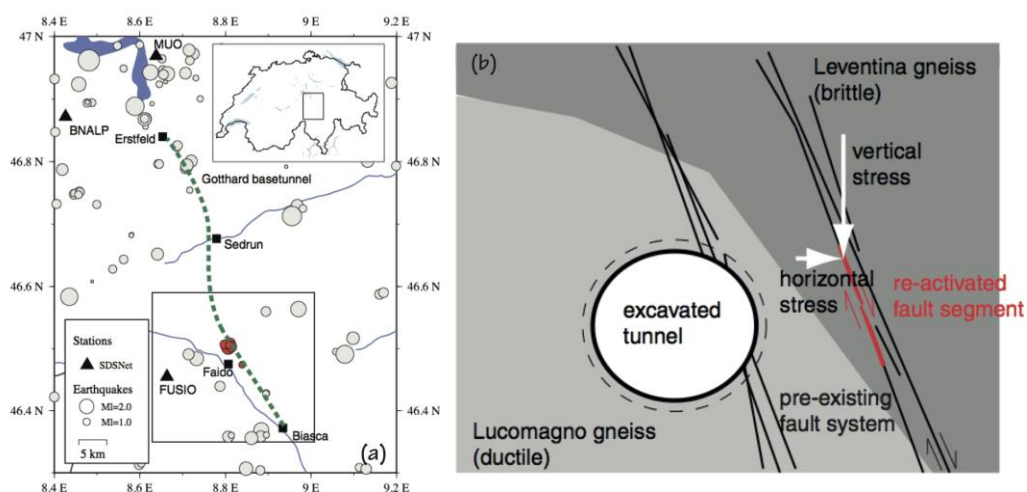


Figure 1. Example of seismicity induced by tunnel excavation: the case of the Gotthard Base Tunnel (October 2005 – August 2007). (a) Map of the area with the red circles indicating the earthquake near Faido. The green dashed line is the base tunnel. (b) Interpretation and conceptual model by Husen et al. (2013). Both figures are taken from the original contribution by Husen et al. (2013), Figure 1 and Figure 18b, respectively.

3. MODELING APPROACH

We idealize a suboptimal condition in which a fault zone strikes parallel to the tunnel excavation direction, in agreement with the geometrical conditions hypothesized by Husen et al. (2013) for the event that occurred at the Gotthard Base Tunnel (Fig. 1b). The stress changes and their evolution during the excavation are evaluated with a numerical continuum Lagrangian solver (FLAC3D, Itasca, 2017). The excavation of tunnel is modeled by assuming a void space with no mechanical properties (null model). At this stage, we neglect the effect of installation of support as well as pore pressure changes due to excavation. The base case scenario is as simple as possible to highlight the physical mechanisms leading to the fault reactivation. The model aims at reproducing the typical conditions for an access tunnel in a nuclear waste repository in clay material, and does not intend to reproduce the conditions for large events such as the one at Gotthard Base Tunnel, which would require a much complex geological representation. The diameter of the tunnel is 10 m and the excavation is assumed to occur at a depth of 500 m with a 2.5 m step in an elastic medium ($K=10$ GPa, $G=3.33$ GPa). All the parameters and conditions are summarized in Table 1, and are similar to values obtained from analysis conducted at Mont Terri (Amann et al., 2018; Urpi et al., 2019), although considering a deeper, and less perturbed state of stress. We have used such properties for the base case simulation in order to have a larger range for the sensitivity analysis compared to the base case.

3.1 Boundary and initial conditions

Figure 2 shows the computational domain with the assumed boundary conditions. We model a three-dimensional domain with dimension $100\text{ m} \times 200\text{ m} \times 200\text{ m}$. We assume initial hydrostatic conditions to account for effective stress, although the fluid flow is neglected during the course of the simulation. The initial vertical stress is assumed lithostatic with a value of 13.24 MPa at depth of the tunnel excavation with a gradient of 26.5 kPa/m. The

initial maximum and minimum horizontal stresses are with ratio $S_H=S_h=0.6S_v$, corresponding to a value of 7.95 MPa (gradient 15.89 kPa/m). Such stress conditions are considered to be representative of a generic geological repository for nuclear waste storage located at 500 m depth (Urpi et al., 2019). For simplicity, we assumed normal stress conditions (i.e. the maximum principal stress vertical σ_v). Such conditions imply that the maximum horizontal stress (σ_H), here in the direction of the excavation, striking as the fault and with the same magnitude as the minimum horizontal stress (σ_h), does not play a major role. The values for the stresses, albeit realistic, are not related to a specific site. Both x -boundaries (at +50/-50 m) have fixed stress conditions, as well as the boundary at $y = 200$ m and top domain ($z = -400$ m). We fix the velocity at the bottom ($z = -600$) and excavation side ($y = 0$ m).

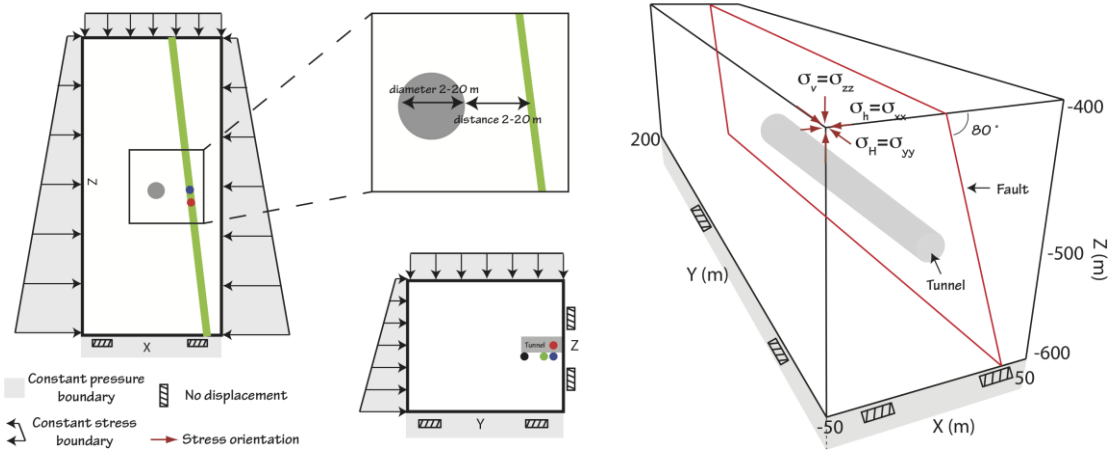


Figure 2. Three-dimensional computational domain. Stress and displacement boundary conditions are shown, as well as the tunnel excavation at the center of the domain. The colored dots indicate the rough position of the monitoring points for the stress evolution.

3.2 Modeling the fault zone reactivation

The numerical modeling setup for the fault zone closely follows several studies on seismicity induced by fluid injection/production accounting for 2D, 3D, as well as fully dynamic simulations (Rutqvist et al., 2016; Zbinden et al., 2017; Rinaldi and Rutqvist, 2019). Here we

account for a quasi-static approach, and the dynamic effects (e.g. wave propagation) are neglected.

The fault zone, dipping 80° , is composed by a 1.4 m elastic damage zone and a 0.6 m core, and it is located at distance of 10 m from tunnel edge. The fault' mechanical behavior is simulated with a ubiquitous joint model, accounting for oriented joint embedded in a Mohr-Coulomb solid. Both joints and matrix could be subjected to plastic strain accumulation, but for sake of simplicity, we set the properties (e.g. cohesion, friction) so that only the joints could be reactivated given critical conditions (Table 1).

We employ an ubiquitous joint model with strain-softening that allows simulating sudden slip on a fault zone with a given orientation because of a frictional law (Rutqvist et al., 2015). For the base case, the friction angle changes from a peak value of 25° to a residual value of 21° with a critical plastic strain of 10^{-7} . The frictional properties are based on recent findings on core sampled at the Main Fault of the Mont Terri Rock Laboratory accounting for a normal stress of about 7 MPa (Orellana et al., 2018).

Both peak (static) and residual (dynamic) friction parameters are highly variable in nature (Zoback, 2007; Ikari et al., 2009; Samuelson and Spiers, 2012; Kohli and Zoback, 2013). For the base case, we assume some reasonable value for a weak fault: the frictional coefficient varies from 0.45 to 0.4. The critical plastic strain relates to the “seismological” critical slip distance of few decimal of micron. This is realistic if we aim at simulating tiny events with an average slip of few tens of micron. This parameter could span several orders of magnitude (Ohnaka, 2003) and it could depend on conditions at the fault (Scuderi and Collettini, 2016).

If the fault is reactivated, we can evaluate the equivalent energy (scalar seismic moment) of a seismic event resulting from the same slip area and average slip on it. The scalar seismic moment is $M_0 = GAd$, where A is the area of the ruptured patch p (including one mesh element or more), G is the shear modulus of the rock, and d is the average slip on the patch.

Finally, empirical relationships allow for calculating an equivalent seismic magnitude as

$$M_w = \frac{2}{3} \log_{10} M_0 - 6.1 \text{ (Kanamori and Anderson, 1975; Kanamori and Brodsky, 2004).}$$

Table 1. Base case initial conditions, host rock, and fault properties. Initial conditions and host rock properties are representative of generic conditions for clay material at 500 m depth.

| INITIAL CONDITIONS AND HOST ROCK PROPERTIES | |
|---|---------------------------------|
| Vertical stress (σ_v) gradient | 26.5 kPa/m (13.24 MPa at 500 m) |
| Maximum horizontal stress (σ_H) gradient | 15.89 kPa/m (7.95 at 500 m) |
| Minimum horizontal stress (σ_h) gradient | 15.89 kPa/m (7.95 MPa at 500 m) |
| Pore pressure gradient | 9.81 kPa/m (4.9 MPa at 500 m) |
| Bulk Modulus (K) | 10 GPa (variable) |
| Shear modulus (G) | 3.333 GPa (variable) |
| Rock density (ρ_R) | 2700 kg/m ³ |
| FAULT PROPERTIES | |
| Dip angle ($^\circ$) | 80 $^\circ$ |
| Bulk modulus (K_f) | 10 GPa (variable) |
| Shear modulus (G_f) | 3.333 GPa (variable) |
| Matrix cohesion (C_m) ^(a) | 1 GPa |
| Matrix Tensile Strength (T_m) ^(a) | 1 GPa |
| Matrix friction angle (ϕ_m) ^(a) | 75 $^\circ$ |
| Joint Peak Cohesion (C_j) ^(a) | 0 |
| Joint Residual Cohesion (C_j^{res}) ^(a) | 0 |
| Joint Tensile strength (T_j) ^(a) | 0 |
| Joint Peak Friction angle (ϕ_j) ^(b) | 25 $^\circ$ (variable) |
| Joint Residual Friction angle (ϕ_j^{res}) ^(b) | 21 $^\circ$ (variable) |
| Joint dilation (ψ) ^(a) | 0 $^\circ$ |
| Critical Plastic strain (ϵ_p^{crit}) ^(c) | 10 ⁻⁷ (variable) |

^(a) Similar to previous works (Rutqvist et al., 2016), these properties were set to prevent reactivation of the fault matrix, whit slip occurring only on joint within the fault zone.

^(b) The friction properties for the fault zone are based literature values. (Orellana et al., 2018)

^(c) The critical plastic strain is based on numerical analysis performed in previous paper (Urpi et al., 2016; Rinaldi and Rutqvist, 2019)

4. RESULTS

4.1 Base case results

In the following section, we present the results of a base-case simulation. Figure 3 shows the evolution of the stress conditions (normal effective and shear stress) at four different location on the fault zone. As soon as the excavation starts at $y = 0$, the region next to the excavation undergoes decrease in normal stress (red, blue, and green lines), while the farther regions are

subjected to an increase in normal effective stress (black line). The more the excavation front is close to a monitoring point, the larger the variation expected in that excavation step. When the conditions approach failure (red dashed line in Fig. 3), the reactivation of the fault occurs, and the shear stress at the monitoring point drops. In the figure, the reactivation occurs at a point located at $y = 11.25$ m and $z = -7$ m (i.e. below the tunnel surface), while the

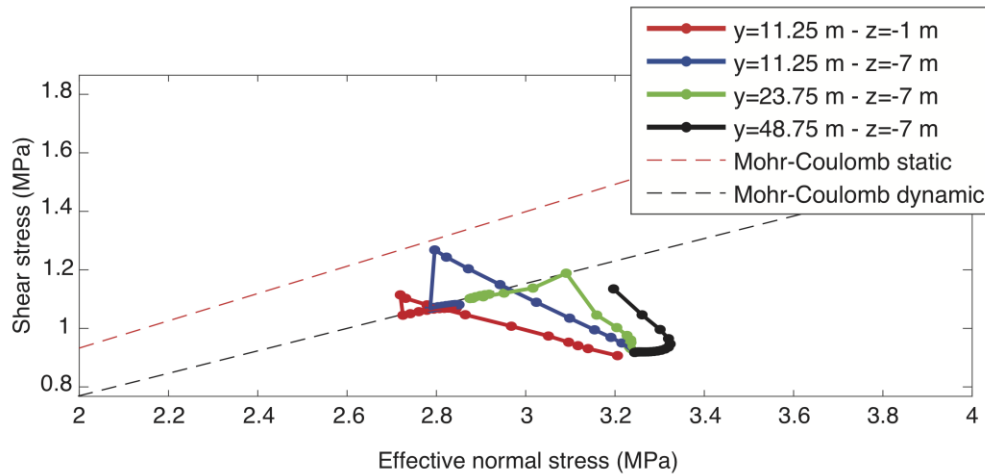


Figure 3. Evolution of the stress path at four different location. The monitoring points are located all within the fault and their exact location is in the label. Fig. 2 shows the location of the colored with respect to the tunnel.

excavation front is at $y = 25$ m. Such reactivation causes a shear stress drop that depends on the frictional properties of the fault zone (Table 1).

Figure 4 shows the distribution of the shear and normal effective stress on the fault zone and their variation upon reactivation. On the fault zone, the shear stress is symmetric with respect to the depth of the tunnel, with an increase (decrease) in the region at a depth above (below) the excavation. The normal stress changes evolution is different. Indeed a greater variation is observed at about ten meters above depth of the tunnel excavation. Both stresses mostly present variation behind the excavation front ($y = 22.5$).

As observed in the stress path (Fig 3), the reactivation of the fault causes a stress drop. Fig. 4c shows quite clearly the region affected by this drop. The new excavation step causes two effects: (1) a continuous elastic variation; (2) the reactivation of the fault. The shear stress

changes present both effects, as the region at depth shallower than the tunnel presents mostly elastic variation, while the stress drop is located in a region up to 20 m below the tunnel excavation. As the reactivation of the fault does not result in a large variation of the normal stress (Fig. 3), the changes in Fig. 4d are mostly elastic. Fig. 4c,d both show that the stress changes, although less than 0.1 MPa, can extend for few tens of meters in the regions ahead the excavation front. Worth to note some minor effect of the boundary at $y = 0$ m for the normal stress changes (Fig. 4d).

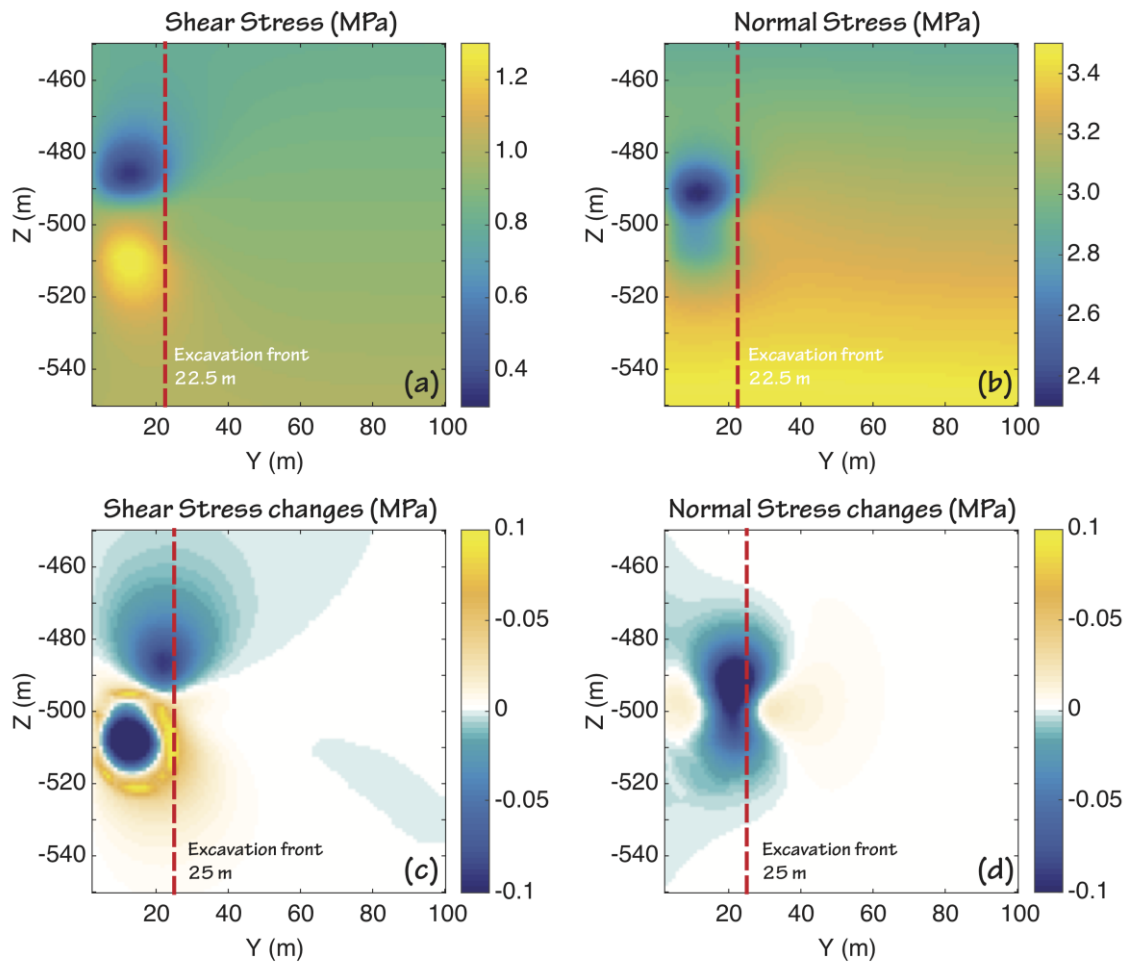


Figure 4. (a,b) Distribution of shear stress and normal effective stress before reactivation, respectively. The red dashed line represent the front of the excavation ($y = 22.5$ m). (c,d) Shear and normal stress changes after fault reactivation. The red dashed line represent the front of the excavation ($y = 25$ m).

The pattern of the plastic strain accumulation gives a better understanding of the results in terms of possible seismic fault reactivation. We observed a variation of plastic strain over a total area of about 400 m² (Fig. 5a). The maximum plastic strain is 0.5×10^{-3} , which is quite larger than the assumed critical plastic strain, but still small enough to results in only few micron slip at the fault. Assuming the reactivation is seismic, with the average slip on the ruptured patch of 5 μm , it would correspond to an earthquake of magnitude $M_w = -1.5$. While the excavation continues, a larger region is reactivated up to a total area of about 1200 m² at 50 m of excavation (Fig. 5b). The accumulated plastic strain also increases to a maximum of 10^{-3} , but with a smaller slip when averaged in the entire ruptured area. The equivalent moment magnitude would be slightly larger if this entire area is ruptured at once ($M_w = -1.27$).

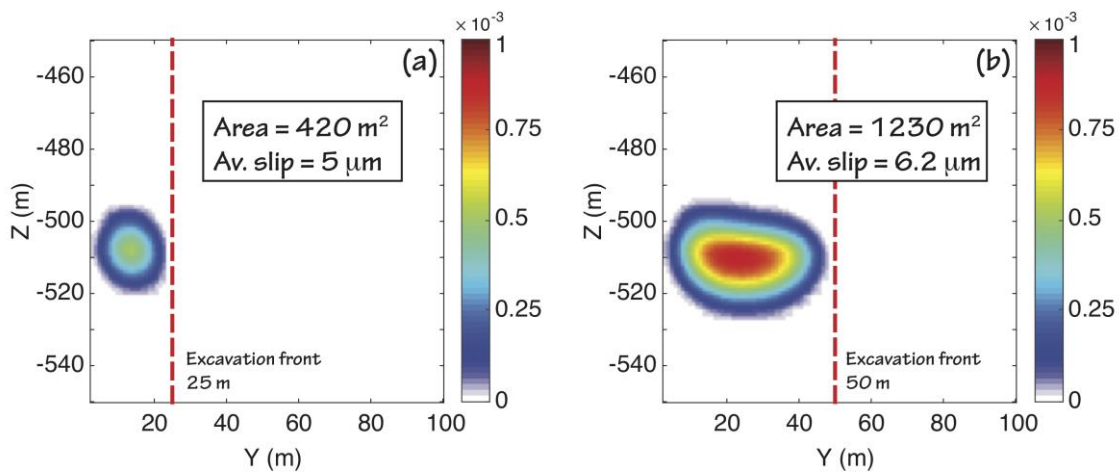


Figure 5. (a) Distribution of plastic shear strain at the time of reactivation. The red dashed line represent the front of the excavation ($y = 25$ m). (b) Distribution of plastic shear strain after 50 m of excavation. The red dashed line represent the front of the excavation.

4.2 Sensitivity analysis

In this section, we investigate the effect of changing some of the parameters in the base case scenario. On the one hand, we investigate how the rupture area and the average slip on fault vary when changing frictional properties, rock elastic properties, as well as the stress conditions. On the other hand, we investigate on the maximum peak and minimum residual

that reactivate the fault as function of the tunnel size and distance fault-tunnel. For the latter analyses the fault not necessarily reactivates, and it is worth investigate if the reactivation could occur with “realistic” fault frictional parameters.

4.2.1 Frictional properties of the fault

Figure 6 shows the variation of the total ruptured area and the average slip on fault after 50 m of excavation. The critical plastic strain does not play a big role if lower than 10^{-4} as the area and the average slip present only minor variations in the analyzed range (Fig. 6a). Worth to mention that the fault does not reactivate if the critical plastic strain is higher than 10^{-4} for the specific stress conditions and peak friction in the base case scenario. This behavior is explained because the excavation is causing an amount of deformation that depends only on the amount of rock being removed. If the critical plastic strain is lower that this deformation, plastic reactivation occurs, independently on the exact value. However, if this critical plastic strain is too high, the frictional drop may be not full and the rupture localized to a small patch. To properly address this transition, however, a full dynamic simulation would be needed, which is out of the scope of the current paper.

Changing the peak friction angle has a larger effect on rupture area and slip (Fig. 6b). The larger the friction angle, the more stress is required to reach reactivation, resulting then in a larger average slip (red line), which is then distributed on a smaller area (blue line). The average slip varies between 1-10 μm in the peak friction angle range $20\text{-}25^\circ$. The rupture area after 50 m of excavation decreases from about 6000 m^2 to about 1000 m^2 .

Changes in residual friction angle affect even more the fault reactivation (Fig. 6c). The average slip presents a minimum of about 1 μm at around 17° (red line), while the rupture area decrease monotonically from about 6000 m^2 to 600 m^2 in the range $15\text{-}23^\circ$ (blue line).

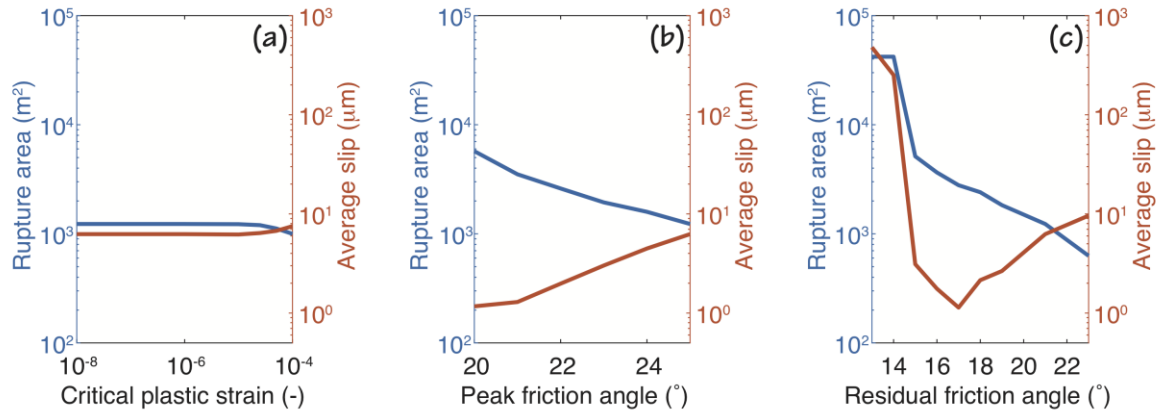


Figure 6. Rupture area and average slip as function of critical plastic strain (a), peak/static friction angle (b), and residual/dynamic friction angle (c) after 50 m of tunnel excavation

Quite interestingly, if the residual friction angle is smaller than 15° the fault reactivation results in a so-called “runaway rupture” (i.e. a rupture that extend for the entire length of the fault – 40000 m^2) with average slip in the order of hundreds of micron. Such runaway rupture is a numerical instability in the simulator, which to solve the balance equation need to propagate the rupture to the whole fault.

4.2.2 Stress conditions and rock properties

The stress conditions applied for the base case scenario represent already a critically stressed environment. Figure 7a shows how the rupture area and the average slip changes when further reducing the ratio between horizontal and vertical stress. Quite interestingly, the more stressed is the fault, the lower the resulting average slip, the larger the rupture area. This is explained by the fact that the reactivation occurs earlier if the stress ratio is lower, not allowing then to build up enough stress along the rupture area, which can be larger as it is easier to reactivate the fault. However, if the stress ratio is small enough, a runaway rupture occurs, similarly to what happens for low residual friction angle. In the case of low stress ratio, however, the resulting slip is smaller, although the entire fault ruptures. Assuming a

stress ratio lower than 0.55 will result, for the given frictional conditions, in a rupture at initial condition (i.e. before excavation).

Figure 7b shows the changes in rupture area and average slip as function of the elastic properties (bulk modulus). As the figure shows, the rupture area is constant and not affected by the changes in elastic properties (blue line), while the average slip highly depends on the value chosen and it can be as large as few hundreds of micron for very soft rock (red line). This behavior is easily explained by the fact that we impose a stress change condition at the excavation front, resulting then independent from the elastic properties. Consequently, the rupture area does not change as it relates only to the value of stress at reactivation, but the average slip depends on deformation and hence highly affected by changes in elastic properties.

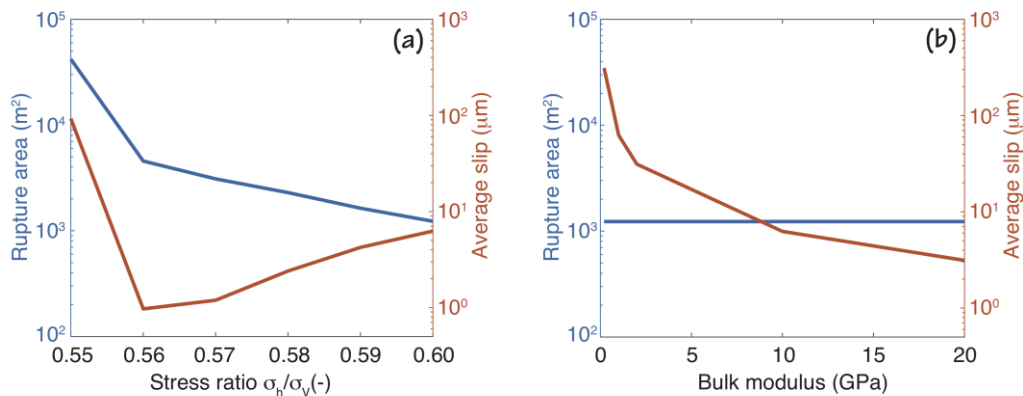


Figure 7. Rupture area and average slip as function of stress ration (a), and bulk modulus (b) after 50 m of tunnel excavation

4.2.3 Tunnel size and fault distance

We evaluate the peak friction needed to reactivate the fault and the residual friction to avoid runaway rupture as function of the tunnel diameter and distance tunnel-fault.

In the case of tunnel size, the fault is always at fixed 10 m distance. The smaller the tunnel being excavated, the smaller the stress changes on the fault, the smaller the peak friction angle for the reactivation (Fig. 8a). The peak friction changes from 16.4° for a diameter of 2

m to 41° for a 20 m-wide tunnel. Interestingly, the smaller the peak friction, the smaller the difference with the residual friction to prevent runaway rupture. For a 2 m-wide tunnel, such a difference is only 0.7° (i.e. the residual is 15.7°) and increases up to 30.8° for a 20 m-wide tunnel (i.e. the residual is 10.2°). This result indicate that is extremely hard to reactivate a fault zone when excavating a tunnel with small diameter, and if this happens the fault is critically stressed and is very easy to induced “large” runaway events in the model. Similarly, the sensitivity analysis on the tunnel-fault distance shows that is very hard to reactivate a fault zone that is located far from the tunnel. For this set of simulations, we vary the distance tunnel-fault and keep the dimeter of the tunnel at 10 m. The larger the distance, the smaller the peak friction angle, the smaller the difference peak-residual (Fig. 8b). The peak angle is 41° with residual at 9.4° when the fault is at 5 m distance and decreases to 18.8° with residual at 15.4° when the distance is 20 m. Quite interesting is the case of a fault only 2 m away from the tunnel face: the reactivation occurs with values much larger than 45° , the upper boundary for most rocks in nature. Fixing then the upper boundary, we need to scale the cohesion to 2 MPa to have reactivation at 45° peak friction. Such cohesion, however, prevents the fault from a runaway rupture even in case of extremely low residual friction angle (1°).

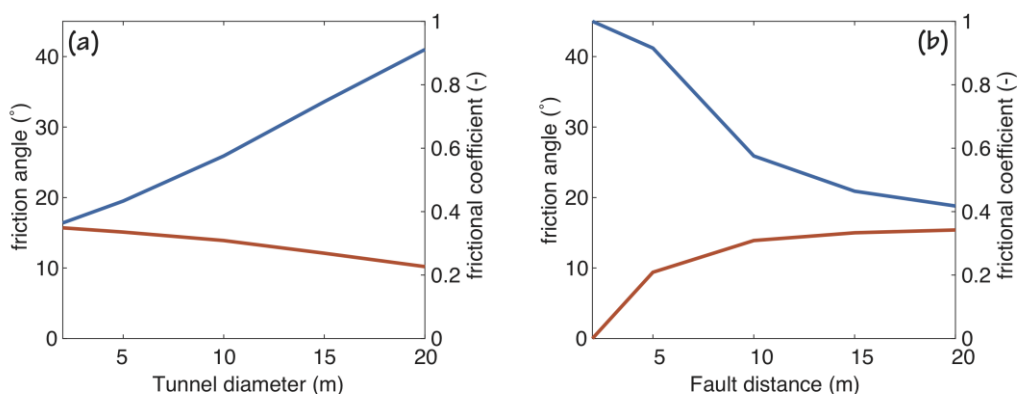


Figure 8. Peak and residual friction angle (frictional coefficient) as function of the tunnel diameter (a) and distance tunnel-fault (b)

4.2.4 The case of multiple, small tunnels

In this section, we focus on a simulation with multiple tunnels, following the Swiss-concept for deep geological repository (NAGRA, 2016). By assuming typical clay rock properties, we model the excavation of three tunnels with diameter 2 m and with an *inter-tunnel* distance of 40 m. The fault zone has the same properties as the base case above, and is placed at a distance of 10 m from wall of tunnel 2 (Fig. 9a). During excavation of the tunnels we monitor the stress evolution at two points placed on the fault plane (red and blue points in Fig. 2). Results show that the stress changes due to the small tunnels are not critical and the fault is not reactivated. Figure 9b shows that most of the changes in stress are due to the excavation of the Tunnel 2 for both monitoring points (blue lines), while little stress changes occur for excavation of Tunnels 1 and 3 (red and green lines). The excavation of Tunnel 2 causes some stress changes, but the variation does not bring to critical condition necessary for reactivation (dashed, black line in Fig. 3b).

The results above highlight that the risk of induced seismicity can be evaluated by looking only at the tunnel closest to the fault. Hence, critical parameters (e.g. peak and residual frictional angle) or conditions (e.g. stress state) could theoretically reactivate the fault and potentially result in a runaway rupture. As an example, for the 2 m tunnel, as highlighted above, this can be simulated if the peak and friction angle are smaller than 16° (frictional coefficient 0.28).

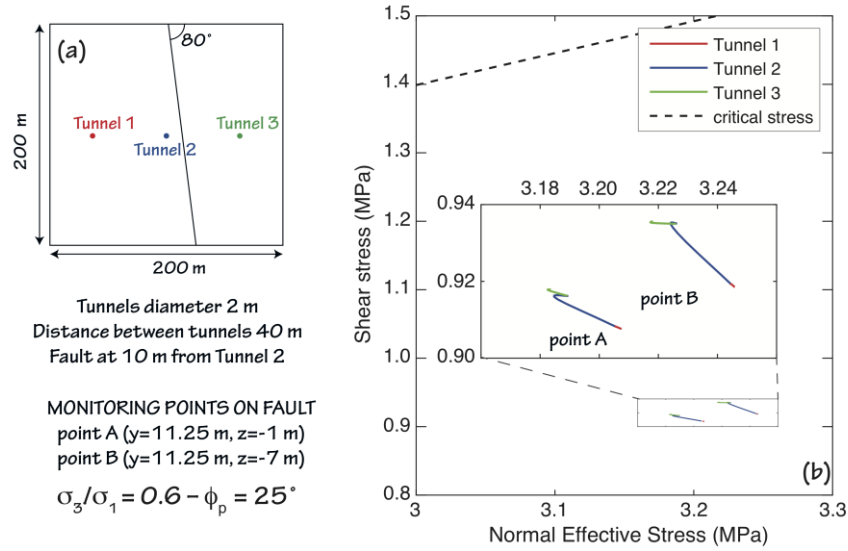


Figure 9. Effect of multiple small tunnels in Clay material. (a) Tunnels positions with respect to fault. (c) Stress path for two points located on the fault plane.

5. CONCLUSION

Some examples in literature show that damaging seismicity can indeed be induced by tunnel excavation and constitute a risk to be evaluated during the construction phase of a deep geological repository, independently of the rock type. Modern, faster mechanized tunneling techniques tend to destabilize the stress conditions in a shorter time and, as a consequence, to increase the risk of induced seismicity. This aspect needs to be considered in the planning phase. However, compared to mining-induced seismicity, there are large differences in observed event magnitudes, probably related to the different excavation depths (few hundreds of meters vs. several kilometers for mining). Hence, the existing criteria for mining vibrations could not be useful, unless re-adapted to the scale relevant for tunneling and for the construction of a deep geological repository.

The numerical model, presented here, shows that the reactivation of a fault zone due to tunnelling in clay material is possible, but resulting mostly in minor seismicity (if any). For a tunnel with size similar to an access tunnel for nuclear repository, a relatively large event can only be induced if the state of stress is critical, or if the frictional properties of the fault are

extremely low. The possible cases of reactivation are even reduced for small tunnels (e.g. emplacement tunnels), and the excavation of multiple, small tunnels does not increase substantially the amount of stress changes on a nearby fault zone. In the worst-case conditions, however, the fault could still reactivate with a runaway rupture extending to the whole fault. From a numerical modelling perspective, a runaway rupture is only limited by the size of the fault itself, but in nature the presence of natural barriers or heterogeneities in frictional properties. Indeed, while in the current model we always use a weakening law for the friction, results highlight that the clay material is rather aseismic, undergoing frictional strengthening during slip (Orellana et al., 2018).

Given the uncertainties in measurements of stress state and rock properties at depth, their large small-scale variations, and the immature understanding of the underlying processes, a maximum possible magnitude cannot be established by numerical modelling only. A detailed analysis of the geological conditions and analysis of frictional properties, combined with numerical modelling, are essential to estimate the seismic risk during the construction of a deep geological repository for nuclear waste disposal.

In the case of clay, our results and previous frictional analysis show that the potential to reactivate fault in clay is small. However, it is worth to note that a detailed analysis of induced seismicity during excavation can provide a further characterization of the repository rock allowing, for example, to locate planes of weakness and to assess their stability and geometry (e.g. Saari, 1999). Knowing the exact position of fault zones could be relevant at later stages of a nuclear waste repository during which other physical processes (e.g. thermal pressurization) may induced the fault reactivation (Urpi et al., 2019).

434

435 **ACKNOWLEDGMENTS**

436 This work was supported by a research agreement between the SED and the Swiss Federal
 437 Nuclear Safety Inspector (ENSI). A. P. Rinaldi was partly financed by a SNSF Ambizione
 438 Energy grant (PZENP2_160555). We thank Thomas van Stiphout and Ernando Saraiva
 439 (ENSI) for useful comments on a preliminary version of the manuscript. Comments from two
 440 anonymous reviewer and the editor are all greatly appreciated.

441

442 **REFERENCES**

- 443 Amann, F., Gonidec, Y. Le, Senis, M., Gschwind, S., Wassermann, J., Nussbaum, C., Sarout,
 444 J., 2018. Analysis of acoustic emissions recorded during a mine-by experiment in an
 445 underground research laboratory in clay shales. *Int. J. Rock Mech. Min. Sci.* 106, 51–59.
 446 doi:10.1016/j.ijrmms.2018.04.021
- 447 Anagnostou, G., 1995. The influence of tunnel excavation on the hydraulic head. *Int. J.*
 448 *Numer. Anal. Methods Geomech.* 19, 725–746. doi:10.1002/nag.1610191005
- 449 Chou, W.-I., Bobet, A., 2002. Predictions of ground deformations in shallow tunnels in clay.
 450 *Tunn. Undergr. Sp. Technol.* 17, 3–19. doi:10.1016/S0886-7798(01)00068-2
- 451 Ellsworth, W.L., Llenos, A.L., McGarr, A.F., Michael, A.J., Rubinstein, J.L., Mueller, C.S.,
 452 Petersen, M.D., Calais, E., 2015. Increasing seismicity in the U. S. midcontinent:
 453 Implications for earthquake hazard. *Lead. Edge* 34, 618–626.
 454 doi:10.1190/tle34060618.1
- 455 Giraud, A., Picard, J.M., Rousset, G., 1993. Time dependent behavior of tunnels excavated in
 456 porous mass. *Int. J. Rock Mech. Min. Sci. Geomech. Abstr.* 30, 1453–1459.
 457 doi:10.1016/0148-9062(93)90137-3
- 458 Gonidec, Y. Le, Sarout, J., Wassermann, J., Nussbaum, C., 2014. Damage initiation and
 459 propagation assessed from stress-induced 126–139. doi:10.1093/gji/ggu122
- 460 Grigoli, F., Cesca, S., Rinaldi, A.P., Manconi, A., López-Comino, J.A., Clinton, J.F.,
 461 Westaway, R., Cauzzi, C., Dahm, T., Wiemer, S., 2018. The November 2017 M_w 5.5
 462 Pohang earthquake: A possible case of induced seismicity in South Korea. *Science (80-*
 463 *)*. 360, 1003–1006. doi:10.1126/science.aat2010
- 464 Grigoli, F., Cesca, S., Priolo, E., Rinaldi, A.P., Clinton, J.F., Stabile, T.A., Dost, B.,
 465 Fernandez, M.G., Wiemer, S., Dahm, T., 2017. Current challenges in monitoring,
 466 discrimination, and management of induced seismicity related to underground industrial
 467 activities: A European perspective. *Rev. Geophys.* 55, 310–340.
 468 doi:10.1002/2016RG000542
- 469 Guglielmi, Y., Cappa, F., Lançon, H., Janowczyk, J.B., Rutqvist, J., Tsang, C.F., Wang,
 470 J.S.Y., 2013. ISRM Suggested Method for Step-Rate Injection Method for Fracture In-
 471 Situ Properties (SIMFIP): Using a 3-Components Borehole Deformation Sensor, in: The
 472 ISRM Suggested Methods for Rock Characterization, Testing and Monitoring: 2007-
 473 2014. Springer International Publishing, Cham, pp. 179–186. doi:10.1007/978-3-319-
 474 07713-0_14
- 475 Husen, S., Kissling, E., von Deschanden, A., 2013. Induced seismicity during the
 476 construction of the Gotthard Base Tunnel, Switzerland: hypocenter locations and source
 477 dimensions. *J. Seismol.* 17, 63–81. doi:10.1007/s10950-012-9313-8
- 478 Ikari, M.J., Saffer, D.M., Marone, C., 2009. Frictional and hydrologic properties of clay-rich

- fault gouge. *J. Geophys. Res. Solid Earth* 114. doi:10.1029/2008JB006089
- Itasca, 2017. FLAC3d V6.0, Fast Lagrangian Analysis of Continua in 3 Dimensions, User's Guide.
- Kanamori, H., Anderson, D.L., 1975. Theoretical basis of some empirical relations in seismology. *Bull. Seismol. Soc. Am.* 65, 1073–1095. doi:??
- Kanamori, H., Brodsky, E.E., 2004. The physics of earthquakes. *Reports Prog. Phys.* 67, 1429–1496. doi:10.1088/0034-4885/67/8/R03
- Khademian, Z., Poeck, E., Garvey, R., Ozbay, U., 2016. Studies of Seismicity Generated by Unstable Failures around Circular Excavations, in: 50th US Rock Mechanics / Geomechanics Symposium.
- Kohli, A.H., Zoback, M.D., 2013. Frictional properties of shale reservoir rocks. *J. Geophys. Res. Solid Earth* 118, 5109–5125. doi:10.1002/jgrb.50346
- Langenbruch, C., Zoback, M.D., 2016. How will induced seismicity in Oklahoma respond to decreased saltwater injection rates? *Sci. Adv.* 2, e1601542–e1601542. doi:10.1126/sciadv.1601542
- Loew, S., Lützenkirchen, V., Hansmann, J., Ryf, A., Guntli, P., 2015. Transient surface deformations caused by the Gotthard Base Tunnel. *Int. J. Rock Mech. Min. Sci.* 75, 82–101. doi:10.1016/j.ijrmms.2014.12.009
- Lu, C., Liu, Bin, Liu, Biao, Liu, Y., Wang, H., Zhang, H., 2019. Anatomy of mining-induced fault slip and a triggered rockburst. *Bull. Eng. Geol. Environ.* doi:10.1007/s10064-019-01464-8
- Martin, C.D., Chandler, N.A., 1996. The Potential for Vault-Induced Seismicity in Nuclear Fuel Waste Disposal: Experience from Canadian Mines Possibilities 20.
- Martino, J.B., Chandler, N.A., 2004. Excavation-induced damage studies at the Underground Research Laboratory. *Int. J. Rock Mech. Min. Sci.* 41, 1413–1426. doi:10.1016/j.ijrmms.2004.09.010
- McGarr, A., Simpson, D., Seeber, L., 2002. Case histories of induced and triggered seismicity. *Int. Geophys.* 81, 647–661. doi:10.1016/S0074-6142(02)80243-1
- Mezger, F., Anagnostou, G., Ziegler, H., 2013. The excavation-induced convergences in the Sedrun section of the Gotthard Base Tunnel. *Tunn. Undergr. Sp. Technol. Inc. Trenchless Technol. Res.* 38, 447–463. doi:10.1016/j.tust.2013.07.016
- NAGRA, 2016. Technical report 14-13: High-level waste repository-induced effects.
- Ohnaka, M., 2003. A constitutive scaling law and a unified comprehension for frictional slip failure, shear fracture of intact rock, and earthquake rupture. *J. Geophys. Res. Solid Earth* 108. doi:10.1029/2000JB000123
- Orellana, L.F., Scuderi, M.M., Collettini, C., Violay, M., 2018. Frictional Properties of Opalinus Clay: Implications for Nuclear Waste Storage. *J. Geophys. Res. Solid Earth* 123, 157–175. doi:10.1002/2017JB014931
- Preisig, G., Dematteis, A., Torri, R., Monin, N., Milnes, E., Perrochet, P., 2014. Modelling Discharge Rates and Ground Settlement Induced by Tunnel Excavation. *Rock Mech. Rock Eng.* 47, 869–884. doi:10.1007/s00603-012-0357-4
- Quick, H., Bergmeister, K., Facchin, E., Michael, J., 2010. Aicha-Mauls on the Brenner Base Tunnel - status of the works and results / . Aicha-Mauls am Brenner Basistunnel - Stand der Arbeiten und Ergebnisse. *Geomech. Tunn.* 3, 520–533. doi:10.1002/geot.201000044
- Rinaldi, A.P., Rutqvist, J., 2019. Joint opening or hydroshearing? Analyzing a fracture zone stimulation at Fenton Hill. *Geothermics* 77, 83–98. doi:10.1016/j.geothermics.2018.08.006
- Rutqvist, J., Børgesson, L., Chijimatsu, M., Hernelind, J., Jing, L., Kobayashi, A., Nguyen, S., 2009. Modeling of damage, permeability changes and pressure responses during excavation of the TSX tunnel in granitic rock at URL, Canada. *Environ. Geol.* 57, 1263–

1274. doi:10.1007/s00254-008-1515-6
- Rutqvist, J., Rinaldi, A.P., Cappa, F., Jeanne, P., Mazzoldi, A., Urpi, L., Guglielmi, Y., Vilarrasa, V., 2016. Fault activation and induced seismicity in geological carbon storage – Lessons learned from recent modeling studies. *J. Rock Mech. Geotech. Eng.* 8, 789–804. doi:10.1016/j.jrmge.2016.09.001
- Rutqvist, J., Rinaldi, A.P., Cappa, F., Moridis, G.J., 2015. Modeling of fault activation and seismicity by injection directly into a fault zone associated with hydraulic fracturing of shale-gas reservoirs. *J. Pet. Sci. Eng.* 127, 377–386. doi:10.1016/j.petrol.2015.01.019
- Saari, J., 1999. An overview of possible applications of microearthquake monitoring at the repository site of spent nuclear fuel in Finland.
- Samuelson, J., Spiers, C.J., 2012. Fault friction and slip stability not affected by CO₂ storage: Evidence from short-term laboratory experiments on North Sea reservoir sandstones and caprocks. *Int. J. Greenh. Gas Control* 11, S78–S90. doi:10.1016/j.ijggc.2012.09.018
- Scuderi, M.M., Collettini, C., 2016. The role of fluid pressure in induced vs. triggered seismicity: insights from rock deformation experiments on carbonates. *Sci. Rep.* 6, 24852. doi:10.1038/srep24852
- Stiros, S.C., Kontogianni, V.A., 2009. Coulomb stress changes: From earthquakes to underground excavation failures. *Int. J. Rock Mech. Min. Sci.* 46, 182–187. doi:10.1016/j.ijrmms.2008.09.013
- Suckale, J., 2009. Induced Seismicity in Hydrocarbon Fields. *Adv. Geophys.* 51, 55–106. doi:10.1016/S0065-2687(09)05107-3
- Urpi, L., Rinaldi, A.P., Rutqvist, J., Wiemer, S., 2019. Fault reactivation induced by thermal pressurization and stress transfer around a deep geological repository in a clay formation. *J. Geophys. Res.* submitted.
- Urpi, L., Rinaldi, A.P., Rutqvist, J., Cappa, F., Spiers, C.J., 2016. Dynamic simulation of CO₂-injection-induced fault rupture with slip-rate dependent friction coefficient. *Geomech. Energy Environ.* 7, 47–65. doi:10.1016/j.gete.2016.04.003
- Zbinden, D., Rinaldi, A.P., Urpi, L., Wiemer, S., 2017. On the physics-based processes behind production-induced seismicity in natural gas fields. *J. Geophys. Res. Solid Earth* 122, 3792–3812. doi:10.1002/2017JB014003
- Zhao, X., Cai, Meifeng, Cai, M., 2010. Considerations of rock dilation on modeling failure and deformation of hard rocks — a case study of the mine-by test tunnel in Canada. *J. Rock Mech. Geotech. Eng.* 2, 338–349. doi:10.3724/SP.J.1235.2010.00338
- Zoback, M.D., 2007. Reservoir Geomechanics, First edition.